Cross sections for electron scattering from magnesium

Oleg Zatsarinny* and Klaus Bartschat†
Department of Physics and Astronomy, Drake University, Des Moines, Iowa 50311, USA

Sergey Gedeon, Viktor Gedeon, Vladimir Lazur, and Elizabeth Nagy
Department of Theoretical Physics, Uzhgorod State University, Uzhgorod 88000, Ukraine
(Received 10 February 2009; published 26 May 2009)

A *B*-spline *R*-matrix (close-coupling) method has been used to perform a systematic study of angle-differential cross sections for electron scattering from neutral magnesium. The calculations cover elastic scattering and excitation of the five excited states $(3s3p)\ ^{3,1}P^o$, $(3s3d)\ ^1D$, $(3s4s)\ ^1S$, and $(3s4p)\ ^1P^o$. A multiconfiguration Hartree-Fock method with nonorthogonal orbitals was employed for an accurate representation of the target wave functions. The close-coupling expansion for the collision problem included 37 bound states of neutral magnesium. Angle-differential cross sections are presented for incident electron energies from 10 to 100 eV. These results, as well as the corresponding angle-integrated cross sections, are compared with various experimental data and predictions from other close-coupling and distorted-wave calculations. In spite of a few remaining discrepancies, the overall agreement between our results and the experimental data is very satisfactory.

DOI: 10.1103/PhysRevA.79.052709 PACS number(s): 34.80.Dp

I. INTRODUCTION

Several sets of experimental measurements of differential cross sections (DCSs) for electron scattering from neutral Mg were published recently [1–6]. Along with earlier works [7–9] they provide an excellent opportunity to test various state-of-the-art theoretical methods employed for the calculation of electron-atom collision processes. For example, relative DCSs for elastic scattering and excitation of the $(3s3p)\ ^1P^o$ and $(3s3p)\ ^3P^o$ states at 20 and 40 eV were presented by Brown *et al.* [1,2]. The data were compared with predictions obtained by the convergent close-coupling (CCC) and *R*-matrix with pseudostates (RMPS) methods. The good agreement between experiment and theory regarding the angular dependence of the DCS gave some confidence in putting the experimental data on an absolute scale by normalization to theory. These calculations, along with a study of the electron-induced resonance transition $(3s^2)\ ^1S \rightarrow (3s3p)\ ^1P^o$ [9], are the only extensive close-coupling (CC) calculations available for *e*-Mg collisions.

Most of the recent measurements, on the other hand, were compared with results from either first-order perturbative calculations [10,11] or earlier close-coupling models [12,13]. The small CC expansions used in the latter are unlikely to provide reliable results, except for very low or relatively high energies, i.e., cases where the dominant coupling occurs only between a few channels or channel coupling is small altogether. Indeed, serious discrepancies between experiment and theory, for example, for excitation of higher-lying states such as $(3s4s)\ ^1S$ and $(3s4p)\ ^1P^o$ at 10 and 15 eV [5], call for more extensive theoretical studies of electron scattering from Mg.

Most previous calculations were devoted to selected individual transitions and a few energies. The purpose of the present work, therefore, is to provide a comprehensive set of results that covers essentially all recent experimental data. This systematic comparison of available experimental and theoretical results makes it possible to assess the accuracy of the existing data and to search for possible sources of the discrepancies between experiment and theory. The present calculations were performed with an extended version of the *B*-spline *R*-matrix (BSR) method [14], in which a *B*-spline basis is employed to represent the continuum functions in the close-coupling expansion of the scattering wave function. Recent applications of this method to quasi-two-electron atoms such as Ca [15] and Zn [16] showed considerable improvement over previous calculations in the agreement between experiment and theory for low-energy scattering. The use of nonorthogonal orbital sets, both for the construction of the target wave functions and for the representation of the scattering functions, allowed us to generate more accurate descriptions of the target structure than those used in previous collision calculations. In particular, the present target wave functions account for both the valence and core-valence correlations *ab initio* through multiconfiguration expansions with an open core.

This paper is organized as follows. After outlining the description of the target structure, we summarize the most important aspects of the collision calculations. This is followed by a presentation of the angle-differential cross sections for elastic scattering and for excitation of the $(3s3p)\ ^{1,3}P^o$, $(3s3d)\ ^1D$, $(3s4s)\ ^1S$, and $(3s4p)\ ^1P^o$ states in Mg. Angle-integrated cross sections (ICSs) for these states are presented and discussed as well. Our results are compared with the available experimental data and predictions from other theoretical models. We conclude with a discussion of the remaining discrepancies and an outlook for possible improvements in future theoretical studies.

*oleg_zoi@yahoo.com
†klaus.bartschat@drake.edu

TABLE I. Excitation and binding energies (in eV) for the spectroscopic target states of Mg. The experimental values are derived from the NIST database [19].

Configuration	Term	Excitation	Binding	Theory	Difference
$3s^2$	^1S	0.000	−7.646	−7.527	0.119
$3s3p$	$^3P^o$	2.714	−4.932	−4.882	0.050
$3s3p$	$^1P^o$	4.346	−3.300	−3.241	0.059
$3s4s$	^3S	5.108	−2.538	−2.511	0.027
$3s4s$	^1S	5.394	−2.253	−2.226	0.027
$3s3d$	^1D	5.753	−1.893	−1.887	0.006
$3s4p$	$^3P^o$	5.932	−1.715	−1.705	0.010
$3s3d$	^3D	5.946	−1.700	−1.693	0.007
$3s4p$	$^1P^o$	6.118	−1.528	−1.509	0.019
$3s5s$	^3S	6.431	−1.215	−1.206	0.009
$3s5s$	^1S	6.516	−1.130	−1.12	0.010
$3s4d$	^1D	6.588	−1.058	−1.054	0.004
$3s4d$	^3D	6.719	−0.927	−0.924	0.003
$3s5p$	$^3P^o$	6.726	−0.920	−0.916	0.004
$3s4f$	$^1F^o$	6.779	−0.867	−0.867	0.000
$3s4f$	$^3F^o$	6.779	−0.867	−0.867	0.000
$3s5p$	$^1P^o$	6.783	−0.863	−0.856	0.007
$3s6s$	^3S	6.930	−0.717	−0.712	0.005
$3s6s$	^1S	6.966	−0.680	−0.675	0.005
$3s5d$	^1D	6.981	−0.665	−0.662	0.003
$3s5d$	^3D	7.063	−0.583	−0.581	0.002
$3s6p$	$^3P^o$	7.069	−0.577	−0.575	0.002
$3s5f$	$^1F^o$	7.092	−0.554	−0.554	0.000
$3s5f$	$^3F^o$	7.092	−0.554	−0.554	0.000
$3s6p$	$^1P^o$	7.094	−0.552	−0.549	0.003
$3p^2$	^3P	7.173	−0.473	−0.446	0.027
$3s7s$	^3S	7.173	−0.473	−0.47	0.003
$3s7s$	^1S	7.192	−0.454	−0.449	0.005
$3s6d$	^1D	7.194	−0.452	−0.449	0.003
$3s6d$	^3D	7.246	−0.400	−0.394	0.006
$3s7p$	$^3P^o$	7.250	−0.396	−0.387	0.009
$3s6f$	$^1F^o$	7.262	−0.384	−0.379	0.005
$3s6f$	$^3F^o$	7.262	−0.384	−0.379	0.005
$3s7p$	$^1P^o$	7.263	−0.383	−0.371	0.012
$3s8s$	^3S	7.310	−0.336	−0.302	0.034
$3s8s$	^1S	7.322	−0.325	−0.282	0.043
$3p^2$	^1S	8.465	0.819	0.949	0.130

II. COMPUTATIONAL METHOD

A. Structure calculations

Magnesium with its ground-state configuration $[1s^22s^22p^6](3s^2)\ ^1S$ and singly excited states $[1s^22s^22p^6](3snl)\ ^{3,1}L$ exhibits many similarities to helium; i.e., it can sometimes be viewed as two electrons outside of a doubly ionized Ne-like $[1s^22s^22p^6]$ core. For simplicity, closed shells will be omitted in the notation below. Both valence and core-valence correlation are important for the ground state and the low-lying excited states of Mg. A widely used method of incorporating core-valence correlation is based on applying a semiempirical core-polarization potential. Although such a potential simplifies the calculations significantly and can provide accurate excitation energies and oscillator strengths, the question always remains how well the model potential can simulate *all* core-valence correlations, including nondipole contributions. In the present approach, we therefore chose to include the core-valence correlation *ab initio* by adding target configurations with an excited core. However, direct multiconfiguration Hartree-Fock (MCHF) calculations in this case usually lead

to very large expansions, which can hardly be used in subsequent scattering calculations. For this reason, we used the *B*-spline box-based close-coupling method [17] to generate the target states.

Specifically, the calculation of the target states included the following steps. We started by generating the core orbitals from a Hartree-Fock calculation for Mg^{2+} and then obtained valence $3s$, $3p$, $3d$, and $4s$ orbitals from a frozen-core calculation for Mg^{+}. Next, we simulated the core-valence correlation by adding $2p^5\bar{n}l\bar{n}'l'$ configurations through the expansion

$$\phi(2p^6nl) = a_{n\ell}\phi_{HF}(2p^6nl) + \sum_{\bar{n}l\bar{n}'\bar{l}'} b_{\bar{n}l\bar{n}'l'}\chi(2p^5\bar{n}l\bar{n}'l'), \quad (1)$$

where the bar indicates a correlated rather than a physical orbital. In other words, the Hartree-Fock wave functions $\phi_{HF}(2p^6nl)$ were improved by correlation functions χ with a $2p$-excited core. These calculations were performed with the MCHF code of Froese Fischer *et al.* [18]. Since the mean radii for the $\bar{n}l$ orbitals lie between the mean radii of the core and the valence orbitals, this method allows us to incorporate the core-valence correlation with a relatively small number of configurations (between 10 and 20 in the present case). Note that the correlation orbitals $\bar{n}l$ were optimized for each state separately.

The core-valence-correlated states of Mg^{+} were then used as target states in *B*-spline bound-state close-coupling calculations to generate the low-lying states of atomic Mg. The corresponding multichannel expansion had the structure

$$\begin{aligned}\Phi(2p^63snl,LS) = {} & \mathcal{A}\sum_{nl}\{\phi(2p^63s)P(nl)\}^{LS} \\ & + \mathcal{A}\sum_{nl}\{\phi(2p^63p)P(nl)\}^{LS} \\ & + \mathcal{A}\sum_{nl}\{\phi(2p^63d)P(nl)\}^{LS} \\ & + \mathcal{A}\sum_{nl}\{\phi(2p^64s)P(nl)\}^{LS}, \end{aligned} \quad (2)$$

where $\mathcal{A}$ denotes the antisymmetrization operator. For brevity of the notation, we assume that the expansion coefficients are incorporated in the unknown functions $P(nl)$ for the outer valence electron. These functions were expanded in a *B*-spline basis, and the corresponding equations were solved subject to the condition that the wave functions vanish at the boundary. This scheme yields a set of orthogonal one-electron orbitals for each bound state, but orbitals in different sets are no longer orthogonal to each other. In practice, this procedure is often referred to as using "nonorthogonal orbitals," and we will do so as well. Finally, we used the same multichannel expansion (1) as for the $3snl$ states for all nl^2 states with equivalent electrons. The number of physical states that we can generate in this method depends on the size a of the *R*-matrix box. Choosing $a=80a_0$ (with $a_0=0.529\times10^{-10}$ m denoting the Bohr radius), we obtained a good description for all low-lying states of Mg up to $(3s8s)\ ^1S$.

We included 110 *B* splines of order 8 in the present calculations. Of course, since the above *B*-spline bound-state close-coupling calculations generate different nonorthogonal sets of orbitals for each atomic state, their subsequent use is somewhat complicated. On the other hand, our configuration expansions for the atomic target states only contained between 20 and 50 configurations for each state and hence could be used in the collision calculations with only modest computational resources.

The target states included in the present scattering calculations are given in Table I, where we also compare the calculated binding energies with the experimental values [19]. The overall agreement between experiment and theory is very satisfactory, with the deviations in the energy splitting generally being less than 0.06 eV, except for the lowest $(3s^2)\ ^1S$ and $(3p^2)\ ^1S$ states. Here the correlation corrections are expected to be most important. The $(3p^2)\ ^1S$ state was included for completeness of the CC expansion, because the $3p^2$ configuration makes a large contribution to the ground-state expansion. The accuracy of the present binding energies is close to the accuracy achieved by extensive MCHF calculations [20], and the current structure description represents a substantial improvement over those used in previous scattering calculations.

Another assessment of the quality of our target description can be performed by comparing the results for the oscillator strengths of various transitions with experimental

TABLE II. Oscillator strengths in Mg. The theoretical results were obtained with the length form of the electric dipole operator.

Initial state	Final state	Present	NIST [21]
$(3s^2)^1S$	$(3s3p)\ ^1P^o$	1.738	1.80
	$(3s4p)\ ^1P^o$	0.116	0.113
	$(3s5p)\ ^1P^o$	0.026	0.024
$(3s3p)\ ^3P^o$	$(3s4s)\ ^3S$	0.138	0.136
	$(3s5s)\ ^3S$	0.016	0.016
	$(3s3d)\ ^3D$	0.626	0.594
	$(3s4d)\ ^3D$	0.126	0.120
$(3s3p)\ ^1P^o$	$(3s4s)\ ^1S$	0.158	0.155
	$(3s5s)\ ^1S$	0.007	0.006
	$(3s3d)\ ^1D$	0.252	0.245
	$(3s4d)\ ^1D$	0.108	0.106
$(3s4s)\ ^3S$	$(3s4p)\ ^3P^o$	1.320	1.37
$(3s4s)\ ^1S$	$(3s4p)\ ^1P^o$	1.249	1.16
$(3s3d)\ ^1D$	$(3s4p)\ ^1P^o$	0.138	0.146
$(3s4p)\ ^3P^o$	$(3s3d)\ ^3D$	0.014	0.017
	$(3s5s)\ ^3S$	0.281	0.277
	$(3s4d)\ ^3D$	0.623	0.613
$(3s4p)\ ^1P^o$	$(3s5s)\ ^1S$	0.301	0.296
	$(3s4d)\ ^1D$	0.934	0.934

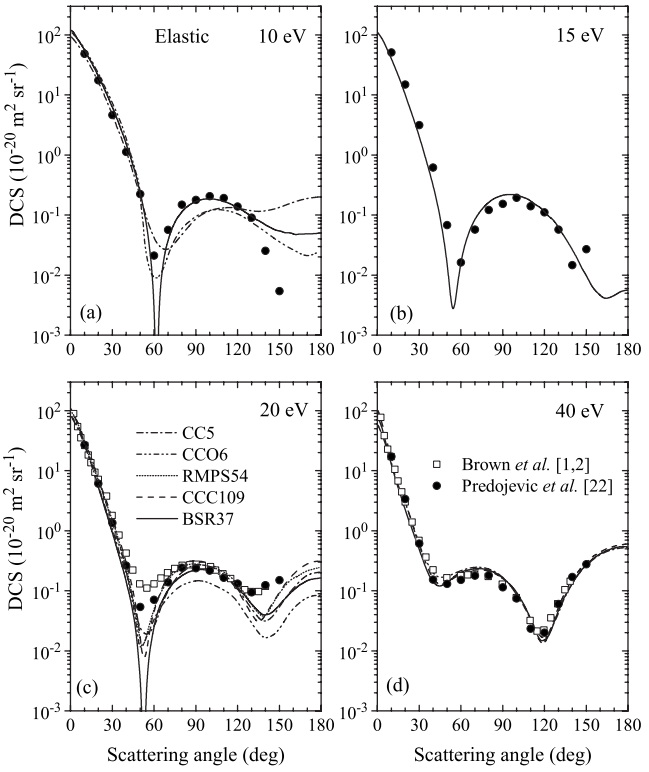

FIG. 1. Angle-differential cross sections for elastic *e*-Mg scattering at impact energies of 10, 15, 20, and 40 eV.

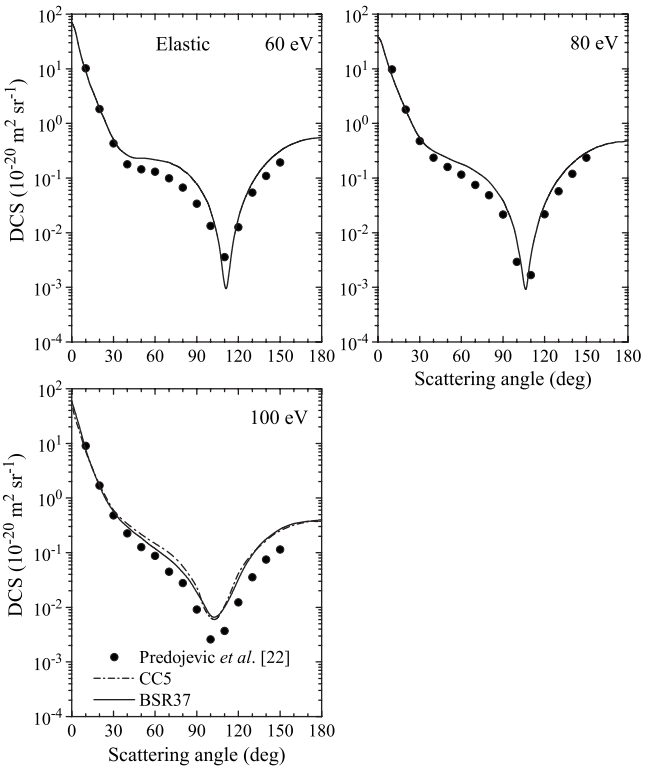

FIG. 2. Angle-differential cross sections for elastic *e*-Mg scattering at impact energies of 60, 80, and 100 eV.

data and other theoretical predictions. Such a comparison is given in Table II with recommended values from the recent critical compilation by NIST [21]. In most cases, we see very close agreement with the values recommended by NIST. There is a small (about 3%) but noticeable discrepancy for the resonance transition $(3s^2)\ ^1S \rightarrow (3s3p)\ ^1P^o$. The NIST value is based on experimental data, although all recent extensive calculations suggest a lower value. For example, very extensive and essentially converged MCHF calculations [20] give $f=1.717$, which is very close to our value. Accurate oscillator strengths are very important to obtain reliable absolute values for both cross sections and rate coefficients for dipole-allowed transitions at high incident electron energies. For low-energy scattering, the accuracy of the oscillator strengths is also important, since it determines whether or not we correctly account for the polarization of the target by the projectile electron.

B. Collision calculations

For the scattering calculations we employed the recently developed *B*-spline *R*-matrix code [14]. Details of this approach, in particular for applications to electron collisions with similar quasi-two-electron targets, can be found in two recent publications on *e*-Ca [15] and *e*-Zn [16] collisions. As mentioned above, the distinctive feature of the method is the use of *B* splines as a universal basis to represent the scattering orbitals in the inner region, $r \leq a$. Hence, the *R*-matrix expansion in this region takes the form

$$\Psi_k^\Gamma(x_1, \ldots, x_{N+1}) = \mathcal{A} \sum_{ij} \bar{\Phi}_i^\Gamma(x_1, \ldots, x_N; \hat{\mathbf{r}}_{N+1}\sigma_{N+1}) \times r_{N+1}^{-1} B_j(r_{N+1}) a_{ijk}^\Gamma. \quad (3)$$

Here the $\bar{\Phi}_i^\Gamma$ are channel functions, while the splines $B_j(r)$ represent the continuum orbitals. The principal advantage of *B*-splines is that they form an effectively complete basis, and hence no Buttle correction to the *R*-matrix is needed in this case. The amplitudes of the wave functions at the boundary, which are required for the evaluation of the *R*-matrix, are given by the coefficient of the last spline, which is the only spline with nonzero value at the boundary.

The other important feature of the present code concerns the orthogonality requirements for the one-electron radial functions. We do not require any orthogonality conditions for the one-electron radial functions used to represent the different target states, and the continuum orbitals do not have to be orthogonal to the bound orbitals either. The use of nonorthogonal orbitals allows us to avoid the introduction of additional $(N+1)$-electron terms in the *R*-matrix expansion. The latter may lead to extensive multiconfiguration expansions, especially when correlated pseudo-orbitals are employed to improve the target states.

The number of *B*-splines and the *R*-matrix radius in the scattering calculations were chosen to be the same as in the calculation of the target bound states. We numerically calculated partial-wave contributions up to $L=50$, followed by a

top-up based on a geometric-series extrapolation if necessary. The cross-section calculations were then carried out in the same way as in standard *R*-matrix calculations.

III. RESULTS AND DISCUSSION

A. Elastic scattering

Figures 1 and 2 show the angle-differential cross sections for elastic scattering of electrons from Mg in its $(3s^2)\ ^1S$ ground state and compare various theoretical predictions with recent experimental data obtained by Brown *et al.* [1,2] and Predojević *et al.* [22]. In addition to the current 37-state *B*-spline *R*-matrix calculations (labeled BSR37), we selected for comparison earlier close-coupling calculations using a 5-state model (CC5) [12] and a 6-state model with optical potential (CCO6) [13], the extensive 109-state convergent close-coupling (CCC109) calculation [9], and a 54-state *R*-matrix with pseudostates (RMPS54) method [1,2].

At an electron-impact energy of 10 eV, all theoretical predictions are in good agreement with the experimental cross sections up to a scattering angle of 130°, with the present results providing the best agreement at intermediate angles between 70° and 130°. However, the two experimental data points at 140° and 150° lie considerably below all theoretical results. Predojević *et al.* [22] used the semiempirical optical-potential calculations of Khare *et al.* [23] (not shown in the figure) to support their results at large angles. These optical-potential calculations yield considerably larger cross sections at small angles than experiment, but after normalizing the experimental DCS at 100° to that theory, they yield good agreement with experiment at large angles. Such support of the experimental data, however, should be taken with care in light of the disagreement at small angles.

At 15 eV, our calculated DCS is in good agreement with experiment [22] at all angles, except for the point at 150°. We are not aware of any other theoretical or experimental DCS data at this energy to compare with. For 40 eV, we notice the closest agreement between the two recent sets of experimental data and the CCC109 and BSR37 results. Consequently, we consider the DCS for this energy to be very well established.

The DCS at 20 eV is the one most frequently found in the literature. The absolute experimental data of Predojević *et al.* [22] agree well with the relative DCS obtained by Brown *et al.* [1], which was visually normalized to the CCC calculation. All theoretical results are in good agreement with experiment and with each other at all angles, except for the two minima observed around 50° and 130°. The calculations predict much deeper minima. While the discrepancies in the first feature may be a result of the finite experimental resolution, Brown *et al.* [1] pointed out that the second minimum predicted by a number of theories is not sufficiently narrow to be explained this way. Also, there is a clear shift in the position of this minimum between experiment (around 130°) and theory (around 140°).

The differential cross sections at 60, 80, and 100 eV are shown in Fig. 2. There is close agreement between the experimental data of Predojević *et al.* [22] and the present calculations for 60 and 80 eV, which are the only results available for comparison at these two energies. The experimental DCS curves exhibit a shoulder and one minimum around $\theta=110°$, whose position is accurately reproduced by our model. We also see reasonable agreement with experiment at 100 eV, although our DCS lies systematically above the experimental data for $\theta>40°$. As expected, due to the diminishing effect of channel coupling at this rather high energy, the present results agree very well with those from the CC5 calculations by Mitroy and McCarthy [12] for all angles.

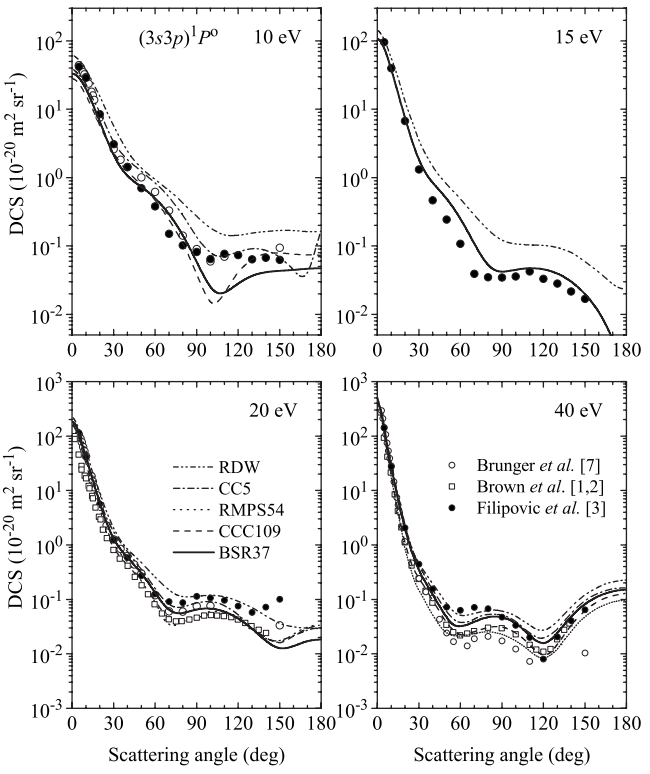

FIG. 3. Angle-differential cross sections for electron-impact excitation of the $(3s3p)\ ^1P^o$ state in Mg at impact energies of 10, 15, 20, and 40 eV.

B. Excitation of the $(3s3p)\ ^1P$ state

The most recent experimental study of the DCS for the $(3s3p)\ ^1P^o$ excitation was presented by Filipović *et al.* [3]. These data, along with the absolute measurements by Brunger *et al.* [7] and relative data of Brown *et al.* [1,2], are compared with the present calculations in Fig. 3. Also included are calculations based on the relativistic distorted-wave (RDW) [3], CC5 [12], RMPS, and CCC [1,2,9] approximations. For the sake of clarity, several earlier experimental and theoretical results (discussed, for example, in [9]) are not shown in the figure.

As expected, the largest spread in the theoretical results is seen for 10 eV. Our DCS agrees most closely with the CCC result, and it is also in good agreement with the experimental data up to scattering angles of 90°. Around 100°, on the other hand, our BSR37 model predicts a local minimum that is not observed in the experiment. Somewhat surprisingly, the closest agreement with experiment in this angular region is pro-

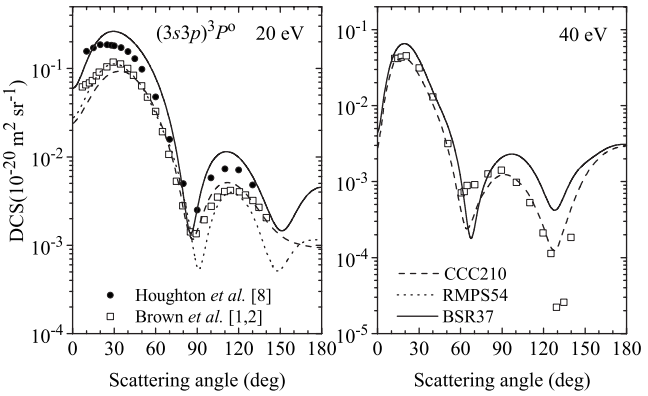

FIG. 4. Angle-differential cross sections for electron-impact excitation of the $(3s3p)\ ^3P^o$ state in Mg for impact energies of 20 and 40 eV. Note that RMPS54 results are only available for 20 eV.

vided by the CC5 calculation, whereas the RDW approximation overestimates the cross sections substantially. At 15 eV only one other calculation (RDW) is available for comparison. Here our results are in very satisfactory agreement with experiment [3], while the RDW model again overestimates the cross sections at large angles.

At 20 eV, all CC calculations agree closely with each other and support the existence of two minima around 70° and 150°. However, the logarithmic scale and the very fast drop in the DCS from the forward direction with increasing scattering angle are somewhat deceiving. As will be seen below, there are actually significant differences in the angle-integrated cross sections among the CC calculations, on the order of 25%. The RDW results are once again noticeably higher than those from the CC theories at large scattering angles. For angles above 90°, our DCSs agree better with the absolute measurements by Brunger *et al.* [7] than with those of Filipović *et al.* [3].

For 40 eV, the measured DCS clearly exhibits two minima around 60° and 120°. Their locations are very well predicted by all theories. However, the differences between the absolute values obtained in the various CC calculations become more noticeable. Our calculations are in better agreement with the recent data by Filipović *et al.* [3] than with the earlier measurements. Filipović *et al.* [3] also provided DCS data for 60, 80, and 100 eV, which are in close agreement with the RDW calculations. For the sake of brevity we do not present the comparison of our data with these results here. We note, however, that our results are in very close agreement with those from the RDW model. This finding is not unexpected, since it again expresses the diminishing effect of channel coupling with increasing collision energy.

C. Excitation of the $(3s3p)\ ^3P^o$ state

A comparison of the DCS for excitation of the $(3s3p)\ ^3P^o$ state is given in Fig. 4. The results for this state exhibit a very different angular dependence and are about 3 orders of magnitude smaller compared to those for elastic scattering and the optically allowed $(3s^2)\ ^1S \rightarrow (3s3p)\ ^1P^o$ transition considered above. The DCS for the $(3s3p)\ ^3P^o$ state has its maximum value around 30°, in contrast to the rapid fall from the forward direction for both elastic scattering and the $(3s3p)\ ^1P^o$ state. There are also two well-defined local minima at large scattering angles. All CC calculations shown here predict a very similar angular dependence for the DCS, but there are substantial differences in the absolute values.

At 20 eV, the present DCS values are in close agreement with the absolute measurements by Houghton *et al.* [8], and we also accurately reproduce the ratio between the two maxima at 30° and 120°. The experimental DCSs of Brown *et al.* [2] exhibit the same overall shape, but were normalized to give a best overall visual fit to the joint CCC and RMPS results. For this state, an even larger CCC calculation, including 210 states [210-state convergent close coupling (CCC210)], was performed. The considerable reduction (up to a factor of 3) in the theoretical DCS at 20 eV has been attributed to the strong influence of continuum channels not included in the earlier calculations. Since the present calculations did not account for coupling to the target continuum either, we cannot assess their influence. A reduction by a factor of up to 3, however, is certainly large. We also note that good agreement with the absolute data by Houghton *et al.* [8] and even earlier measurements by Williams and Trajmar [6] (not shown in the figure) suggest somewhat larger values of the DCS at 20 eV than predicted by RMPS54 and CCC210.

At 40 eV, the agreement of our DCS with the CCC210 results is better, probably due once again to the decreasing importance of channel coupling at this higher energy. Apart from the depths of both minima, the present BSR37 results are in satisfactory agreement with the relative measurements by Brown *et al.* [1]. Nevertheless, the fact that the CCC210 results differ from ours but are in very good agreement with experiment, except for the depth of the second minimum, suggests that channel coupling to the ionization continuum is still not negligible for this optically forbidden transition, especially in angular regions where the DCS is very small.

D. Excitation of the $(3s4p)\ ^1P^o$ state

Figure 5 shows the differential cross sections for excitation of the $(3s4p)\ ^1P^o$ state. At 10 eV, there is only one set of measurements [5] and one previous calculation [12] in the CC5 approximation for comparison. Note that the recent RDW calculations [11] were considered inadequate for such small energies and thus the authors only presented results for higher energies. As seen from the figure, the experimental results disagree substantially with the DCS values predicted by the CC5 model at scattering angles beyond 60°, whereas our results show almost perfect agreement with experiment. The reason is the slow convergence of the CC expansion for this state. Test calculations performed in a nine-state close-coupling approximation, which included all target states up to $(3s4p)\ ^1P^o$, yielded very similar DCS results to the CC5 model of Mitroy and McCarthy [12].

For the impact energy of 20 eV, there are two sets of measurements [5,6] in the literature, and they agree well with each other over the entire angular range. All calculations also agree well with each other and with the experimental data, although there are some differences for scattering angles less

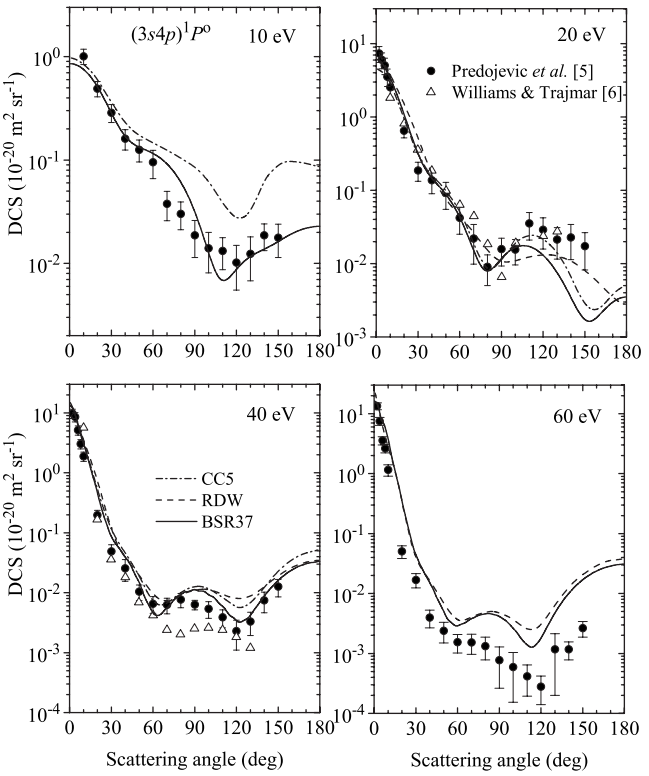

FIG. 5. Angle-differential cross sections for electron-impact excitation of the $(3s4p)\ ^1P^o$ state in Mg for impact energies of 10, 20, 40, and 60 eV.

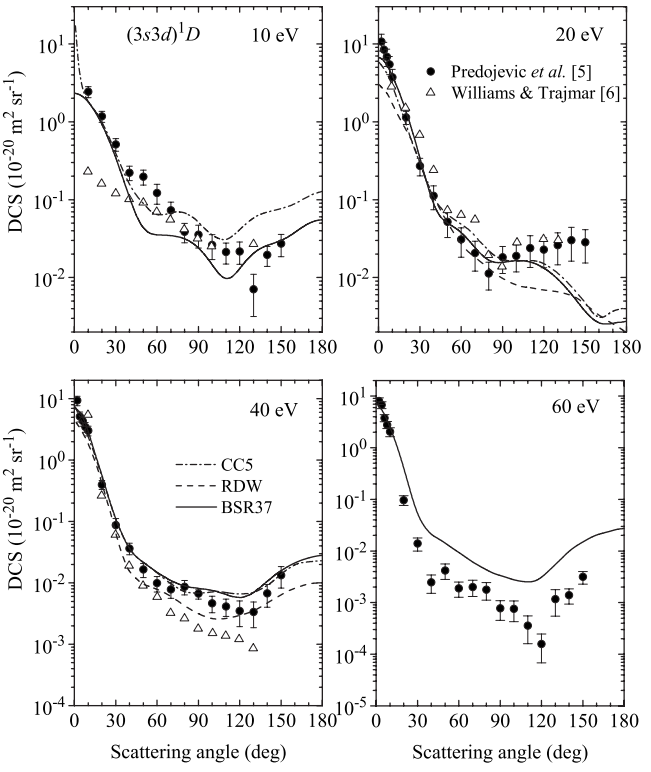

FIG. 6. Angle-differential cross sections for electron-impact excitation of the $(3s3d)\ ^1D$ state in Mg for impact energies of 10, 20, 40, and 60 eV.

than 10° (note the logarithmic scale) and larger than 130°. Near the forward direction, the experimental data lie above the CC5 results, whereas the RDW and the present BSR37 calculations agree very well with each other and experiment. The DCS values at small angles are very important to provide correct angle-integrated cross sections. Both CC calculations predict local minima at 80° and 150°, whereas the RDW model produces only one shallow minimum around 90°. The minimum at 80° obtained in the present calculation is in excellent agreement with the measurements. The second minimum predicted at 150°, on the other hand, is not confirmed by the experimental data, although the size of the error bars shows increasing uncertainty. Nevertheless, the RDW calculations yield the closest agreement with experiment in this angular range.

At 40 eV, the two sets of measurements agree very well for scattering angles smaller than 60°. All calculations yield a similar angular dependence and agree well with the recent measurements by Predojević *et al.* [5] over the entire angular range. In particular, both experiment and theory show two minima around 60° and 120°. Our calculations yield the deepest second minimum, in good agreement with the measurements of Predojević *et al.* [5]. At 60 eV, finally, the shapes of the experimental and theoretical DCS curves are similar in that both show a fast drop from forward scattering to an angle of 60° and the deepest minimum around 115°. However, the measurements lie clearly below the calculations for all scattering angles larger than about 10°.

E. Excitation of the $(3s3d)\ ^1D$ state

Angle-differential cross sections for the excitation of the $(3s3d)\ ^1D$ state are presented in Fig. 6. At 10 eV the present calculations yield reasonable agreement with the measurements of Predojević *et al.* [5] at most angles, except for the region from 50° to 70°. Both experiment and theory exhibit a shoulder here, but the BSR37 results fall significantly below the experimental data. The two sets of measured data agree well with each other for angles larger than 50°. At small angles, on the other hand, the data of Williams and Trajmar [6] are systematically lower than those of Predojević *et al.* [5]. Theory clearly favors the latter measurements. Both close-coupling calculations predict a similar angular dependence, but the present BSR37 results are generally lower for angles larger than 40°. There are also significant differences in the forward peak below 10°.

For 20 eV, the agreement between CC5 and BSR37 is much better. Both measurements also provide similar results and agree very well with the BSR37 prediction between 15° and 110°. At small angles, the experimental data are very forward peaked and considerably exceed all theoretical predictions. At angles larger than 110°, the experimental data are again larger than those calculated in any of the models presented.

The closest agreement between experiment [5] and theory is found for 40 eV. Both close-coupling models yield very similar results, while the RDW numbers are systematically lower for almost all angles. Again, the present calculations, as well as CC5, favor the recent data [5] at large angles,

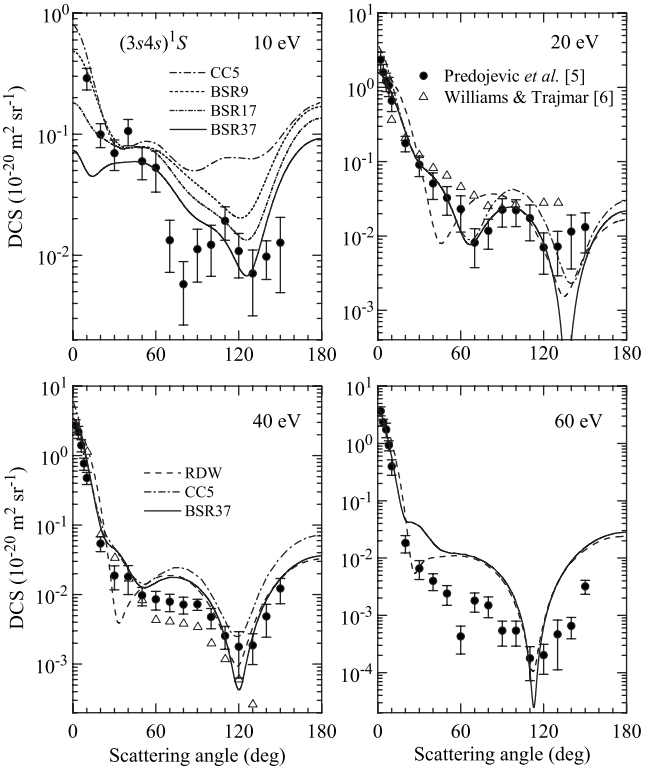

FIG. 7. Angle-differential cross sections for electron-impact excitation of the $(3s4s)\,^1S$ state in Mg for impact energies of 10, 20, 40, and 60 eV.

where they considerably exceed the DCSs from previous measurements [6]. At 60 eV, finally, we only have the measurements published by Predojević *et al.* [5] and the present calculations to compare. The overall agreement resembles the situation for excitation of the $(3s4p)\,^1P^o$ state: the shapes of the experimental and theoretical DCS are similar, but the measured data clearly lie below the calculations for scattering angles larger than 10°.

F. Excitation of the $(3s4s)\,^1S$ state

The excitation of the $(3s4s)\,^1S$ state is the most correlated process considered to date. This excitation is expected to be strongly affected by channel coupling and should strongly depend on the details of the approximation. DCS results for excitation of the $(3s4s)\,^1S$ state are shown in Fig. 7. At 10 eV, the experimental DCS exhibit a complicated structure, which at best qualitatively agrees with the theoretical predictions. The present BSR37 results are considerably lower than those obtained in the CC5 model by Mitroy and McCarthy [12]. In an attempt to shed some light on these discrepancies, we also plot our results obtained with 9-state *B*-spline *R*-matrix (BSR9) and 17-state *B*-spline *R*-matrix (BSR17) close-coupling expansions. Note that the BSR9 results are closest to those from the CC5 model, and the theoretical DCS values decrease systematically with increasing size of the close-coupling expansion. Even our largest model, BSR37, is probably not fully converged with the number of coupled states, but this is the limit of what we can handle with the current code and our available computational resources. Nevertheless, we see satisfactory agreement between experiment and the BSR37 results for a wide range of angles, except for the DCS at angles below 10° and around 80°. We also note the substantial size of the experimental error bars. Such large uncertainties do not allow for final conclusions to be drawn. Instead, more accurate measurements as well as more extensive theoretical calculations are required.

For 20 eV incident energy, the agreement between theory and experiment is much better. The close-coupling calculations accurately reproduce the peak at small angles and the local minimum around 70°, while the RDW model predicts the first minimum around 45°. All calculations also yield a deep minimum near 135°, while the measurements [5] show a more shallow minimum around 125°. At 40 eV, the agreement at small and large angles is even better, with the deep minimum found in the experiment around 120° being reproduced by all theories. However, there is a noticeable disagreement at intermediate scattering angles between 50° and 100°, where all calculations show a local maximum. For 20 eV in particular, but to some extent also at 40 eV, the agreement between the two experimental data sets shown is poor in both shape and magnitude. The calculations generally favor the recent measurements by Predojević *et al.* [5]. Finally, we find good agreement of our BSR37 results with the recent RDW calculations by Sharma *et al.* [11]. However, the theoretical DCS values considerably exceed experiment for angles larger than 20°. The deep minimum predicted around 110° is seen experimentally as well, but not as sharp as a function of the scattering angle.

G. Angle-integrated cross sections

Figure 8 compares the ICSs for the transitions considered above in detail regarding the angular dependence of the DCS. (The results are available in tabular form from the authors upon request.) As seen from the figure, excellent agreement between theory and experiment is found for elastic scattering over the entire energy interval from 10 to 100 eV. This indicates a fast convergence of the theoretical models for this case. This finding differs considerably from the case of small energies around 1 eV, where a strong *p*-wave-shaped resonance was seen experimentally [24]. We also recall the very slow convergence of the close-coupling expansion found in our previous study [25] of low-energy elastic electron scattering from magnesium atoms.

On the other hand, the situation for excitation of the $(3s3p)\,^3P^o$ state is not satisfactory at all. The present calculations agree with the available experimental data at 20 eV, but our results are considerably lower than experiment at 10 eV and considerably higher at 40 eV. An even more extensive CCC210 calculation suggests significantly lower cross sections at 20 and 40 eV, presumably caused by a strong channel-coupling effect to the ionization continuum.

The most frequently studied transition is the $(3s^2)\,^1S \rightarrow (3s3p)\,^1P^o$ excitation. Except for 10 eV, our results agree within the specified error bars with the available experimental data for all energies. Our integrated cross sections are also

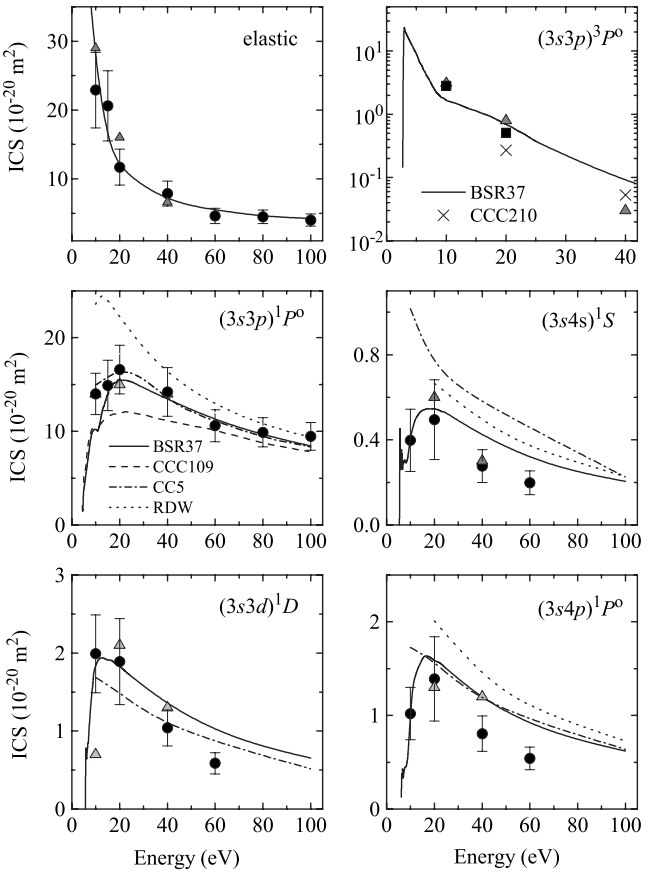

FIG. 8. Angle-integrated cross sections for electron scattering from magnesium in its $(3s^2)\ ^1S$ ground state. The theoretical curves for elastic scattering are indistinguishable within the thickness of the line. Experiment: circles, Predojevic *et al.* [5,22]; triangles, Williams and Trajmar [6].

in good agreement with those from the CC5 calculation and match the RDW results at higher energies. Not surprisingly, the RDW model considerably overestimates the experimental cross section at lower impact energies. The most striking feature is perhaps the much smaller cross sections at low energies obtained in the CCC calculations [9]. This is the most extensive calculation and might be expected to provide the most accurate theoretical data at intermediate energies of a few times the ionization threshold. We note that the CCC cross sections are in very good agreement with the optical measurements by Leep and Gallagher [26], after cascade contributions are accounted for. Filipović *et al.* [3] also compared their results with the optical measurements, and the good agreement was taken as additional support of their data. However, the optical cross sections include significant cascade contributions (about 10% at low energies), and thus the comparison provided is questionable. In light of the large differences between the BSR37 the CCC109 results, additional studies of the low-energy regime seem necessary before the $(3s3p)\ ^1P^o$ cross section can be finalized.

For the higher-lying states, $(3s4s)\ ^1S$, $(3s3d)\ ^1D$, and $(3s4p)\ ^1P^o$, the agreement with the experimental data reveals a similar pattern. We see good agreement at low energies, but the present calculations considerably overshoot the measured cross sections at 40 and 60 eV. Interestingly, the CC5 model also overestimates the cross sections for excitation of the $(3s4s)\ ^1S$ excitation, while it lies below most of the experimental data for the $(3s3d)\ ^1D$ state and agrees very well with the present results (except for the point at 10 eV) for the $(3s4p)\ ^1P^o$ state. The recent RDW results for the $(3s4s)\ ^1S$ and $(3s4p)\ ^1P^o$ states noticeably exceed our cross sections. Overall, the existing theoretical results are consistent with our calculation at higher energies.

IV. SUMMARY

We have presented theoretical results for angle-differential and angle-integrated cross sections for elastic and inelastic electron scatterings from Mg atoms. Unlike in most previous publications on this topic, the numerous experimental data were compared to results obtained using a single highly sophisticated theoretical model. Such a systematic comparison of experimental and theoretical data allowed us to assess the accuracy of the existing data and, where discrepancies persist, suggest areas for further studies.

The calculations were performed with a recently extended version of the *R*-matrix (close-coupling) method [14], in which a *B*-spline basis is employed to represent the continuum functions of the projectile. The use of nonorthogonal orbital sets, both for the construction of the target wave functions and for the representation of the scattering functions, made it possible to generate more accurate descriptions of the target states than those typically used in collision calculations. In particular, the present target wave functions account for both the valence and core-valence correlations *ab initio* through multiconfiguration expansions with an open core.

The present angle-differential and angle-integrated cross sections for elastic scattering are in very good agreement with recent measurements by Predojević *et al.* [22] for a wide range of energies, including recent results at 15, 60, and 80 eV, for which no comparison with theory has been available to date. For the strong dipole-allowed excitation of the $(3s3p)\ ^1P^o$ state, our angle-differential cross sections are in good agreement with existing DCS measurements and, in particular, provide noticeable improvement for the predicted DCS at 15 eV. At the same time, there is considerable disagreement with extensive CCC calculations [9] regarding the angle-integrated cross section at small and intermediate energies. These discrepancies require further studies regarding the convergence of the close-coupling expansion. For the spin-forbidden excitation of the $(3s3p)\ ^3P^o$ state, both the experimental and theoretical data are somewhat scattered. This can partly be attributed to the fact that the cross sections are relatively small and both the target description and channel-coupling effects, including coupling to the ionization continuum, are expected to be important for this transition.

Excitation of the higher-lying $(3s4s)\ ^1S$, $(3s3d)\ ^1D$, and $(3s4p)\ ^1P^o$ states in Mg presents another sensitive testbed for theory. For the angle-integrated cross sections, we found good agreement with experiment for small energies between 10 and 20 eV, but there was a noticeable and unexpected

disagreement at the higher energies of 40 and 60 eV. We suggest this energy region as a candidate for further careful studies, both experimentally and theoretically. Overall we obtained considerable improvement in the agreement with experiment compared to previous CC5 [12] and RDW [11] calculations for these states, especially at low energies.

Finally, excitation of the $(3s4s)\ ^1S$ state turned out to be a major challenge for theory. Channel-coupling effects were found to be extremely important for this transition. Although we obtained considerable improvement in the angle-differential cross section at 10 eV, our CC expansion, and hence our calculations based on that expansion, is likely not fully converged with the number of coupled states. Consequently, even more extensive calculations are highly desirable. Such calculations will require the parallelization of our present computer codes. Work in this direction is currently in progress.

ACKNOWLEDGMENT

This work was supported by the United States National Science Foundation under Grants No. PHY-0555226 and No. PHY-0757755.

[1] D. O. Brown, D. Cvejanović, and A. Crowe, J. Phys. B **36**, 3411 (2003).
[2] D. O. Brown, A. Crowe, D. V. Fursa, I. Bray, and K. Bartschat, J. Phys. B **38**, 4123 (2005).
[3] D. M. Filipović, B. Predojević, V. Pejčev, D. Šević, B. P. Marinković, R. Srivastava, and A. D. Stauffer, J. Phys. B **39**, 2583 (2006).
[4] D. M. Filipović, B. Predojević, D. Šević, V. Pejčev, B. P. Marinković, R. Srivastava, and A. D. Stauffer, Int. J. Mass Spectrom. **251**, 66 (2006).
[5] B. Predojević, V. Pejčev, D. M. Filipović, D. Šević, and B. P. Marinković, J. Phys. B **41**, 015202 (2008).
[6] W. Williams and S. Trajmar, J. Phys. B **11**, 2021 (1978).
[7] M. J. Brunger, J. L. Riley, R. E. Scholten, and P. J. O. Teubner, J. Phys. B **21**, 1639 (1988).
[8] R. K. Houghton, M. J. Brunger, G. Shent, and P. J. O. Teubner, J. Phys. B **27**, 3573 (1994).
[9] D. V. Fursa and I. Bray, Phys. Rev. A **63**, 032708 (2001).
[10] R. Srivastava, R. P. McEachran, and A. D. Stauffer, J. Phys. B **34**, 2071 (2001).
[11] L. Sharma, R. Srivastava, and A. D. Stauffer, Phys. Rev. A **78**, 014701 (2008).
[12] J. Mitroy and I. E. McCarthy, J. Phys. B **22**, 641 (1989).
[13] I. E. McCarthy, K. Ratnavelu, and Y. Zhou, J. Phys. B **22**, 2597 (1989).
[14] O. Zatsarinny, Comput. Phys. Commun. **174**, 273 (2006).
[15] O. Zatsarinny, K. Bartschat, S. Gedeon, V. Gedeon, and V. Lazur, Phys. Rev. A **74**, 052708 (2006).
[16] O. Zatsarinny and K. Bartschat, Phys. Rev. A **71**, 022716 (2005).
[17] O. Zatsarinny and C. Froese Fischer, J. Phys. B **35**, 4669 (2002).
[18] C. Froese Fischer, T. Brage, and P. Jönsson, *Computational Atomic Structure: An MCHF Approach* (Institute of Physics, Bristol, 1997).
[19] Yu. Ralchenko, A. E. Kramida, J. Reader, and NIST ASD Team, NIST Atomic Spectra Database, version 3.1.5, National Institute of Standards and Technology, Gaithersburg, MD, 2008 (http://physics.nist.gov/asd3).
[20] P. Jönsson, C. Froese Fischer, and M. R. Godefroid, J. Phys. B **32**, 1233 (1999).
[21] D. E. Kelleher and L. I. Podobedova, J. Phys. Chem. Ref. Data **37**, 267 (2008).
[22] B. Predojević, V. Pejčev, D. M. Filipović, D. Šević, and B. P. Marinković, J. Phys. B **40**, 1853 (2007).
[23] S. P. Khare, A. Kumar, and L. Kusum, J. Phys. B **16**, 4419 (1983).
[24] N. I. Romanyuk, O. B. Shpenik, A. I. Zhukov, and I. P. Zapesochnyi, Pis'ma Zh. Tekh. Fiz. **6**, 877 (1980).
[25] K. Bartschat, O. Zatsarinny, I. Bray, D. V. Fursa, and A. T. Stelbovics, J. Phys. B **37**, 2617 (2004).
[26] D. Leep and A. Gallagher, Phys. Rev. A **13**, 148 (1976).